Polymer Degradation and Stability 248 (2026) 112065

Contents lists available at ScienceDirect

Polymer Degradation and Stability

journal homepage: www.journals.elsevier.com/polymer-degradation-and-stability

Enhanced pH-responsive 5-FU release from electrospun PLA/PEG fibers incorporating a fluorinated covalent organic framework

Hasinah Rafiq, Yu-I Hsu *, Mitsuharu Suzuki, Supritha Muppuri, Ken-Ichi Nakayama, Hiroshi Uyama *

Department of Applied Chemistry, Graduate School of Engineering, The University of Osaka, 2-1 Yamadaoka, Suita, Osaka 565-0871, Japan

ARTICLE INFO

Keywords:
Electrospinning
Bio-based polymers
PLA/PEG fibers
Fluorinated covalent organic framework
5-fluorouracil
ph-responsive release

ABSTRACT

Electrospinning of bio-based poly(lactic acid) (PLA) is a straightforward approach for encapsulating hydrophilic bioactive compounds within biodegradable polymers for sustained release. PLA offers good mechanical properties, biocompatibility, and non-toxic degradation under physiological conditions. However, its intrinsic hydrophobicity hinders the uniform dispersion of hydrophilic drugs, leading to recrystallization, phase separation, and incomplete drug dissolution. In this study, a fluorinated covalent organic framework (COF) was employed as a nanocarrier to encapsulate the hydrophilic anticancer drug, 5-fluorouracil (5-FU), in electrospun PLA fibers containing polyethylene glycol (PEG) as a compatibilizer. The fluorinated COF achieved a 5-FU loading of 65%, enabling efficient drug incorporation in electrospun PLA/PEG fibers, while suppressing drug recrystallization and achieving sustained, pH-responsive release. Compared to directly loaded fibers, the 5-FU@COF/fibers exhibited enhanced cumulative release at acidic pH (pH 5.4) compared to physiological pH (pH 7.4), due to the pH-induced degradation of both the COF and PLA/PEG fibers. Furthermore, embedding 5-FU@COF particles within the fibrous matrix reduced burst release and provided sustained release in aqueous environments. The presence of COF increased the maximum degradation temperature of the fibers, enhancing the thermal stability of the fiber composite. Additionally, the lowered initial degradation temperature of 5-FU/COF fibers at 200 °C relative to drug-free COF/fibers served as a clear indicator of successful drug loading. Overall, these findings establish pH-responsive COF-polymer composites as a sustainable platform for selective anticancer drug delivery in acidic conditions.

1. Introduction

Electrospinning provides a simple approach to form polymeric fibers with high surface area, tunable porosity, and versatile chemical functionality for biomedical, environmental, and electronic applications [1–4]. Among the broad range of electrospinnable polymers, poly(lactic acid) (PLA) is widely used owing to its good mechanical properties and FDA-approved biocompatibility [5]. Its hydrophobic property is often exploited to retain various bioactive compounds for sustained release under aqueous physiological environments [6,7]. In biomedical applications, conventional polymeric materials used in biomedical devices and drug-delivery systems are predominantly sourced from petroleum-derived plastics and usually persist as non-degradable waste after use, adding to the environmental burden of healthcare [8–11]. In contrast, PLA is produced from renewable feedstocks and undergoes degradation into non-toxic metabolites, offering a bio-based route to produce implants and local drug-delivery systems that minimize long-term plastic accumulation [12].

Despite these advantages, encapsulating highly hydrophilic drugs into hydrophobic PLA matrices remains challenging. This limitation is particularly evident for the anticancer agent 5-fluorouracil (5-FU), where polarity mismatch between the hydrophilic drug and the hydrophobic PLA leads to phase separation during electrospinning, resulting in fibers with poor morphology and surface-directed drug migration after solvent evaporation [13–17]. To address this, PLA is frequently electrospun with a minor fraction of polar solvents such as DMSO and DMF to improve 5-FU solvation and reduce recrystallization in the electrospinning solution [18]. However, these solvents are difficult to remove post-electrospinning due to their high boiling points and may compromise biocompatibility. Alternatively, PLA is often blended with hydrophilic polymers and porous drug carriers to enhance intermolecular interactions and improve 5-FU distribution within PLA matrices

* Corresponding authors at: Department of Applied Chemistry, Graduate School of Engineering, Osaka University, 2-1 Yamadaoka, Suita, 565-0871, Japan.
E-mail addresses: yuihsu@chem.eng.osaka-u.ac.jp (Y.-I. Hsu), uyama@chem.eng.osaka-u.ac.jp (H. Uyama).

https://doi.org/10.1016/j.polymdegradstab.2026.112065
Received 15 December 2025; Received in revised form 12 March 2026; Accepted 15 March 2026
Available online 17 March 2026

[19–23].

Beyond conventional drug carriers, porous covalent organic frameworks (COFs) have recently emerged as versatile hosts for therapeutic compounds due to their high specific surface area, structural diversity, and good biocompatibility [24,25]. The reticular nature of COF synthesis allows diverse inclusion of linkers and functional groups within its framework, enabling precise control over pore chemistry. As a result, COFs can be designed to enhance interactions with target molecules, yielding carriers with homogenous drug dispersion, high loading capacity and efficient release behavior. Additionally, COFs are made up of light, metal-free elements, which offer a major advantage over metal-containing porous frameworks, which may induce undesirable toxicity in biomedical use [26]. In particular, fluorinated imine COFs such as DF-TAPB-COF and DF-TATB-COF have been reported to encapsulate and release 5-FU sustainably due to the favorable interactions provided by fluorine-rich porous frameworks [27].

To date, most COFs designed for 5-FU delivery have only been examined in buffers as free nanoparticles, with limited exploration of their use in polymeric scaffolds. The use of fluorinated COFs as a 5-FU carrier in electrospun PLA fibers remains uninvestigated. Herein, we first synthesized a fluorinated COF *via* room temperature synthesis and loaded it with 5-FU to obtain 5-FU@COF. These 5-FU@COFs were further incorporated into PLA electrospun fibers containing PEG-1000 as a compatibilizer to improve fiber formation and hydrophilicity. The resulting 5-FU@COF/fibers exhibited continuous fibrous morphology and avoided the severe phase separation and surface crystallization observed in directly-loaded fibers. Interestingly, the incorporation of 5-FU@COF within the fibers yields enhanced pH-responsive drug release compared to fibers with directly-loaded 5-FU due to the degradation of imine-linked COF and PLA/PEG fibers in acidic conditions. Most importantly, embedding 5-FU@COF within the fibrous matrix reduced the rapid drug release associated with free 5-FU@COF particles, providing a more sustained release pattern. These findings demonstrate that 5-FU@COF can serve as compatibility-bridging carriers for hydrophilic drugs in hydrophobic electrospun systems, offering a practical route for preparing pH-responsive fibrous scaffolds with potential for localized chemotherapy applications. The present strategy enables the development of a pH-responsive drug release system by utilizing bio-based, biodegradable PLA fibers and metal-free porous organic frameworks, contributing towards current efforts to improve the sustainability of advanced biomedical materials.

2. Experimental

2.1. Materials

Special grade 5-fluorouracil (5-FU), acetic acid, tetrahydrofuran, ethanol, dimethylformamide, chloroform, acetone, mesitylene, 1,4-dioxane, and PEG-1000 were purchased from FUJIFILM Wako Pure Chemical Corporation (Tokyo, Japan). 4,4′,4″-(1,3,5-triazine-2,4,6-triyl) trianiline (TAPT) and 2,5-difluoroterephthalaldehyde (DFTA) were purchased from Nacalai Tesque Inc. (Kyoto, Japan). PLA 4060D was purchased from NatureWorks (Minnesota, USA). PBS solutions were purchased from Thermo Fisher Scientific (USA).

2.2. Synthesis of 5-FU@COF

The fluorinated COF were synthesized using 4,4′,4″-(1,3,5-triazine-2,4,6-triyl)trianiline (TAPT) and 2,5-difluoroterephthalaldehyde (DFTA) based on previous reports with slight modifications [28]. Specifically, 1.2 mmol TAPT, 0.8 mmol of DFTA were dispersed in 80 mL of mesitylene:1,4-dioxane (1:1 ratio) *via* sonication for 10 min. Then, 20 mL of 12 M acetic acid was added, and the solution was stirred for 5 min before being left to stand at room temperature for 3 days. The resulting yellow precipitate was collected *via* vacuum filtration and washed consecutively with THF and ethanol before being dried in vacuo at 70 °C for 12 hours.

The activated TAPT-DFTA (100 mg) was added to 20 mL of hexane containing 260 mg of 5-FU. The mixture was stirred at room temperature for 24 hours. The drug-loaded samples were then separated from the hexane mixture through vacuum filtration and washed repeatedly with hexane and hexane: ethanol (9:1) respectively. The drug-loaded COF were then dried under vacuum at 40 °C for 24 hours and denoted as 5-FU@COF.

2.3. Preparation of 5-FU@COF/fibers

The general preparation scheme of 5-FU@COF/fibers is outlined in Fig. 1. Specifically, neat electrospun fibers consisting of 12 wt% PLA and 10 wt% PEG-1000 (relative to PLA) were first prepared by dissolving 240 mg of PLA and 24 mg of PEG-1000 in 2 mL of a chloroform/acetone (9:1, v/v) solvent mixture. Subsequently, 10 wt% 5-FU@COF (26.4 mg, relative to the total polymer mass) was dispersed into the PLA/PEG-1000 solution *via* sonication to obtain the precursor for electrospun fibers incorporating 5-FU@COF. PLA/PEG-1000 fibers with directly loaded 5-FU and COF-only fibers were prepared as control samples, using the same quantities of 5-FU and neat COF as those incorporated in the 5-FU@COF/fibers. For 5-FU/fibers, the 5-FU was first completely dissolved in 100 μL DMF before being added to the electrospinning solution. Electrospinning was carried out by loading each polymer solution into a 5 mL gas-tight syringe and applying a voltage of 17 kV at a tip-to-collector distance of 15 cm. The flow rate was maintained at 1 mL/h, and the fibers were collected on aluminum foil wrapped around a rotating drum at 200 rpm. The composition of each fiber sample is detailed in Table 1 below.

2.4. General characterization

2.4.1. X-ray diffraction (XRD) and surface area analysis

X-ray diffraction (XRD) patterns were collected on a MiniFlex600 diffractometer (Rigaku) equipped with a D/teX Ultra 1D silicon strip detector and a Cu-Kα radiation source operated at 15 mA of tube current and 40 kV of tube voltage. Nitrogen sorption isotherm measurements were performed at 77 K on a BELSORP MINI X surface area and pore size distribution analyzer (MICROTRAC). Immediately before analysis, samples were dried at 70 °C for at least 6 hours using a BELPREP VAC II vacuum degasser (MICROTRAC).

2.4.2. Scanning electron microscopy (SEM)

The morphology of the fibers and COF particles was observed by SEM (Hitachi, SU3500) at an acceleration voltage of 15 kV. The fibers were mounted on aluminum stubs and sputter-coated with a 20 nm gold-palladium layer beforehand. The COF particles were dispersed in ethanol, dropped on carbon tape, and dried at room temperature for 24 h before measurements. The average diameter of the fibers and particles was calculated using the ImageJ software by measuring the width of 50 individual fiber strands/particles at various locations of each sample.

2.4.3. Fourier-transform infrared spectroscopy (FT-IR)

The chemical bonding characteristics of the samples were analyzed by Fourier Transform Infrared (FTIR) spectroscopy using a Nicolet iS5 spectrometer (Thermo Fisher Scientific, Waltham, MA, USA).

2.4.4. Thermal properties

Thermal properties of the samples were analyzed by the thermogravimetric and differential thermal analysis (TGA and TG-DTA) using a HITACHI STA200RV instrument (Hitachi High-Tech Science Co., Tokyo, Japan). Approximately 4–5 mg of each sample was heated from 40 to 700 °C at a rate of 10 °C min^{-1} under a constant nitrogen flow of 100 mL min^{-1}. The weight loss (TG) and the associated heat flow changes (DTA) measurements were obtained simultaneously to determine the thermal stability and phase transition temperatures of the composites .

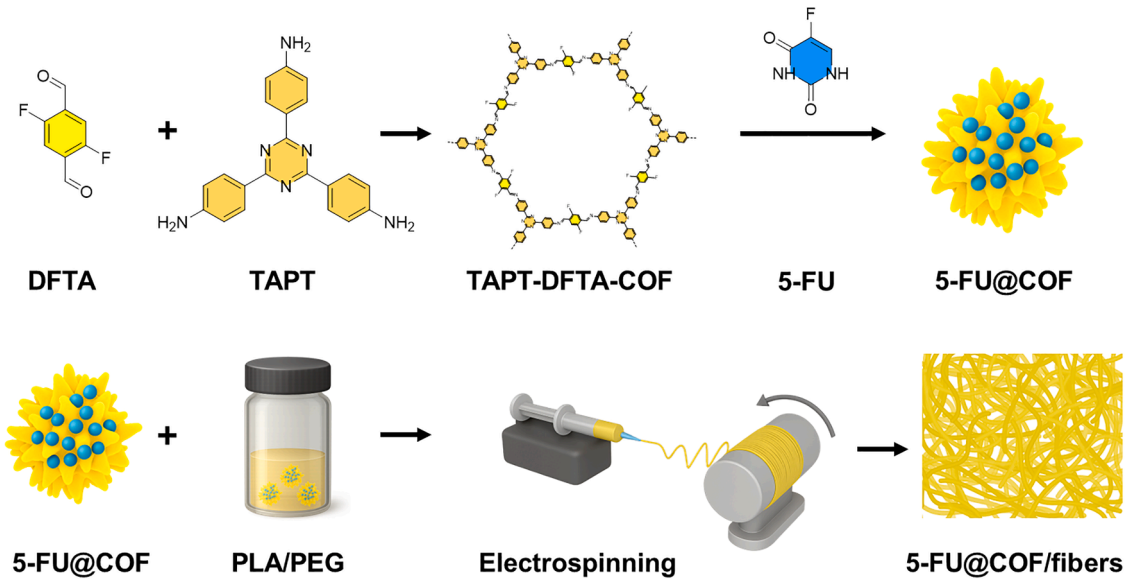

Fig. 1. Schematic illustration of the synthesis of 5-FU@COF and PLA/PEG fibers incorporating 5-FU@COF.

Table 1
Composition of electrospinning solutions for different fiber samples.

Sample	Weight (mg)				
	PLA	PEG-1000	5-FU@COF	COF	5-FU
Fibers	240	24	0	0	0
COF/fibers[a]	240	24	0	9.3	0
5-FU@COF/fibers	240	24	26.4	0	0
5-FU/fibers[b]	240	24	0	0	17.2

[a] COF weight corresponds to the actual COF content (35%) from 26.4 mg 5-FU@COF.
[b] 5-FU weight corresponds to the actual encapsulated 5-FU (65%) from 26.4 mg 5-FU@COF.

Differential scanning calorimetry (DSC) was performed using a HITACHI DSC200 (Hitachi High-Tech Science Co., Tokyo, Japan). 4–5 mg of sample heated from 30 to 300 °C at a rate of 10 °C min^{-1} under a nitrogen flow of 40 mL min^{-1}.

2.4.5. Mechanical properties

Mechanical properties were evaluated using a universal testing machine (EZ Graph, Shimadzu Co., Kyoto, Japan) equipped with a 10 N load cell. Tests were conducted at a strain rate of 20 mm/min, under conditions of 25 °C and 40 % relative humidity, with sample dimensions of 5 × 10 mm. Measurements were done in triplicates for each sample and reported results are expressed as mean ± standard deviation.

2.4.6. Water contact angle and swelling ratio measurement

The surface wettability of the nanofibers was analyzed by the water contact angle (WCA) contact angle goniometer (Drop Master DM300, Kyowa Interface Science Co., Ltd., Saitama, Japan) by applying a 1.0 μL droplet of deionized water onto the fibers. The swelling ratio measurements were performed by immersing the fibers in phosphate-buffered saline (PBS, pH = 7.4 and pH = 5.4) at 37 °C for 24 hours. The samples were then removed, and excess water on their surface was gently blotted with filter paper before weighing. The swelling ratio was calculated using the following equation:

$$Swelling\ ratio(\%) = \frac{M_t - M_o}{M_o} \times 100\% \quad (1)$$

where M_o is the initial weight of fibers, and M_t is the weight of fibers after swelling in PBS for 24 hours. All measurements were done in triplicates for each sample and reported results are expressed as mean ± standard deviation.

2.4.7. Zeta potential measurements

The surface charge of CO and 5-FU@COF were analyzed using the Zeta-potential & Particle size Analyzer ELSZ (Otsuka Electronics, Japan). 1 mg of the samples were dispersed in 5 mL of PBS buffer at pH 7.4 and pH 5.4.All measurements were done in triplicates for each sample and reported results are expressed as mean ± standard deviation.

2.5. Drug loading capacity and in vitro drug release studies

2–3 mg of the drug containing fibers were completely dissolved in 5 mL DMF by heating it at 40 °C for 2 hours. The solution was then filtered using a 0.22 μm filter, and 200 μL of the solution was diluted up to 5 mL PBS 7.4 buffer, and the amount of drug in the sample was measured using a UV–vis spectrophotometer at 266 nm with the help of a calibration curve (Supporting Fig. S1). Measurements were made in triplicates for each sample and reported results are expressed as mean ± standard deviation. Next, the drug loading capacity of the fibers was calculated by the following equation:

$$Drug\ loading\ capacity(\%) = \frac{m_{drug}}{m_{fibers}} \times 100\% \quad (2)$$

Where m_{drug} is the mass of drug extracted from the fiber sample, and m_{fibers} is the total mass of fibers, respectively.

For the drug release studies, 3–4 mg of 5-FU/fibers and 5-FU@COF fibers were placed into 5 mL PBS solution at pH 7.4 and 5.4 under continuous shaking (50 rpm). At set time intervals, 200 μL of the PBS solution was taken and diluted appropriately for UV–Vis measurements at 266 nm. The 5-FU concentration in the withdrawn sample was determined based on calibration curves of the drug in pH 7.4 and pH 5.4 (Supporting Fig. S2). An equal volume of PBS buffer was added to maintain sink conditions. The cumulative release percentage of 5-fluorouracil was calculated according to the following equation:

$$5-FU\ release(\%) = \frac{M_t}{M_n} \times 100\% \quad (3)$$

where M_t denotes the total amount of 5-FU released at time t, and M_n denotes the total amount of 5-FU in the fibers, respectively. Subsequently, the obtained 5-FU release curves were fitted with the

Korsmeyer-Peppas, Higuchi, and Weibull models, respectively:

$$R\,(\%)t = kt^{n} \tag{4}$$

$$R\,(\%)t = kt^{1/2} \tag{5}$$

$$R\,(\%) = R_o\left[1 - \exp\left(-\frac{t}{\alpha}\right)^{\beta}\right] \tag{6}$$

where *R (%) t* denotes the 5-FU release percentage at time *t*, *k* denotes the characteristic kinetics constant, n represents the release exponent for Korsmeyer-Peppas and Higuchi models, while *R (%)* denotes cumulative of drug release, R_o represents maximum drug release of a system (100%), α represents a scale parameter that describes time dependance and β represents the shape of the dissolution curves for Weibull model.

2.6. In vitro degradation test of COF and 5-FU@COF/fibers

The stability of COF at pH 7.4 and pH 5.4 were assessed by immersing 1.5–2.0 mg COF in 2 mL PBS buffers at 37 °C for 24 h. The COF samples were then dried for XRD measurements. The fibrous 5-FU@COF samples were immersed in 5 mL PBS buffer at pH 7.4 and pH 5.4, respectively. At set time intervals, the samples were retrieved, gently rinsed and freeze-dried for SEM analysis. The weight loss % of the samples are calculated based on the equation below:

$$\textit{Weight loss}\,(\%) = \frac{W_1 - W_2}{W_1} \times 100\% \tag{7}$$

where W_1 and W_2 are the weight of fibers before and after degradation, respectively.

3. Results and discussion

3.1. Characterization of 5-FU@COF

The nitrogen adsorption–desorption isotherm of the fluorinated COF exhibited a type-IV profile (Fig. 2a), characteristic of mesoporous materials, with a steep uptake at low relative pressure ($P/P_o < 0.1$) attributed to micropore filling [29,30]. The COF displayed a high BET surface area of 1660 $m^2\ g^{-1}$, estimated from the adsorption fittings (Supporting Fig. S3). XRD patterns (Fig. 2b) confirmed its crystalline structure, showing diffraction peaks at $2\theta = 2.9°$, 5.0°, 5.8°, 7.7°, 10.2°, and 26.1° in accordance with literature data [27]. SEM imaging and size distribution analysis revealed that the COF crystallized into microspherical aggregates with a mean diameter of 4.3 ± 0.7 μm (Fig. 2c,d).

The drug loading capability of the COF was examined through FT-IR, XRD, TGA, and TG-DTA analyses. In the FT-IR spectra (Fig. 3a), a $C = N$ stretching vibration was observed at 1517 cm^{-1} for both pristine COF and 5-FU@COF, indicating that the imine linkage of the framework is preserved after drug incorporation. The characteristic $C = O$ stretching band of 5-FU at 1644 cm^{-1} shifted to 1655 cm^{-1} after loading, reflecting a weakening of the intermolecular hydrogen bonding of 5-FU post encapsulation [31,32]. In Fig. 3b, the XRD patterns of 5-FU@COF displayed diffraction peaks at $2\theta = 2.9°$, 5.0°, 5.8°, and 7.7°, in line with those of the pristine COF, further confirming that the crystalline structure of the COF was preserved after drug loading. Additionally, the main

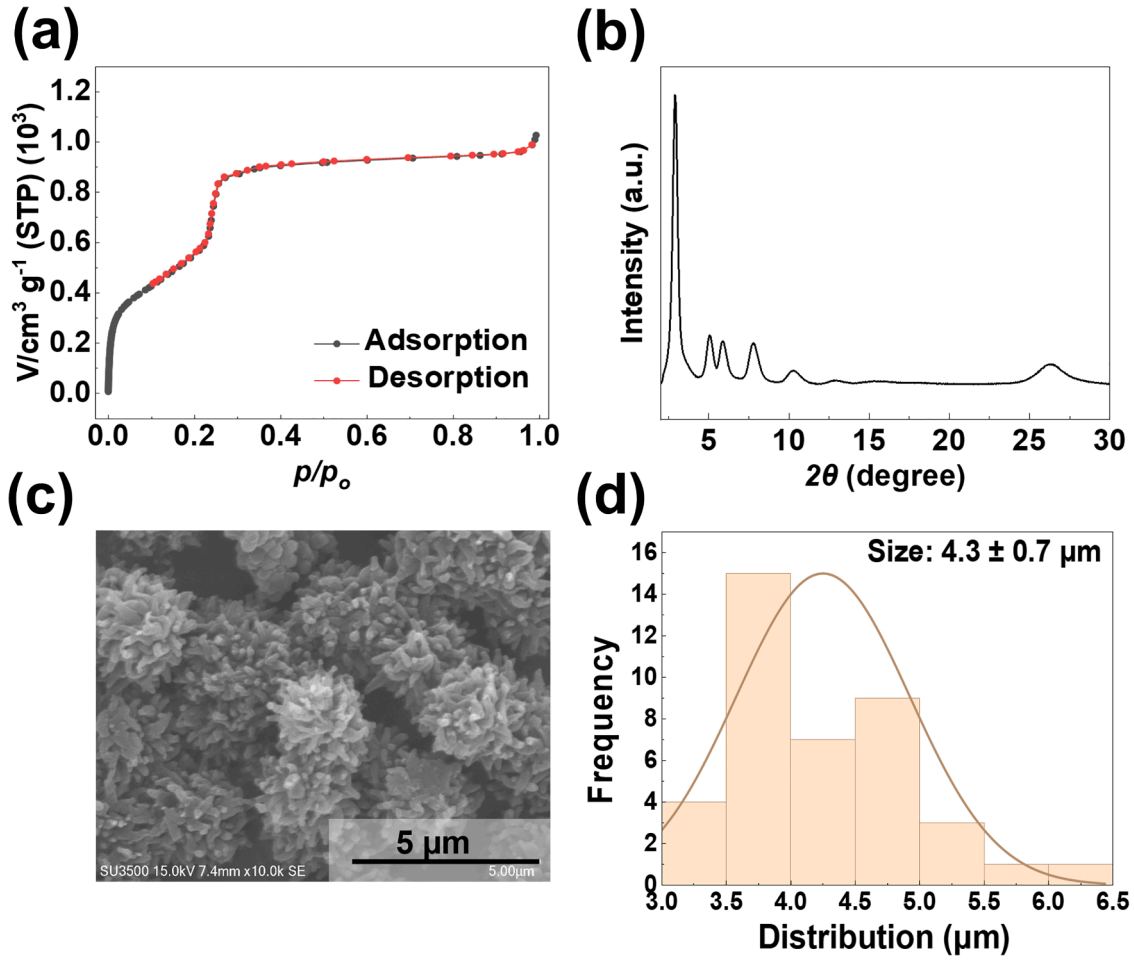

Fig. 2. Nitrogen sorption isotherm at 77 K (a) and XRD patterns (b) of fluorinated COF. SEM images of fluorinated COF at 10,000x magnification (c) and their size distribution (d).

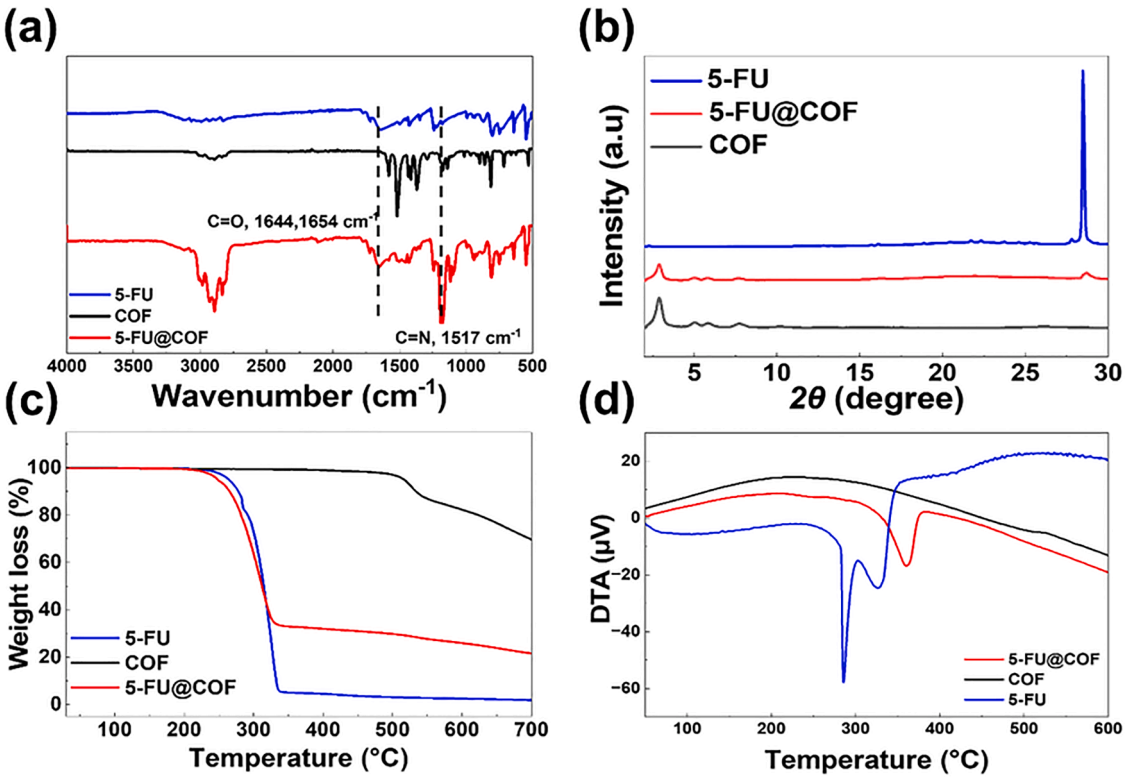

Fig. 3. FT-IR spectra (a), XRD analysis (b), TGA analysis (c), and TG-DTA analysis (d) of 5-FU, COF, and 5-FU@COF.

diffraction peak of 5-FU is present in 5-FU@COF around 28.5° The exact loading capacity of 5-FU@COF was estimated to be 65% based on the thermal degradation of 5-FU in the sample around 200–340 °C (Fig. 3c). TG-DTA analysis (Fig. 3d) was performed to evaluate the thermal behavior of 5-FU adsorbed within the fluorinated COF. The DTA thermogram of pristine 5-FU exhibited two distinct endothermic events at approximately 285 °C and 326 °C, both occurring within the temperature range associated with mass loss in TGA (240 to 352 °C). In contrast, 5-FU@COF displayed a single endothermic event centered at 360 °C. Since this temperature exceeds the degradation range of 5-FU,this peak likely reflects the interaction between decomposed 5-FU products and the COF itself. Furthermore, the COF framework remained thermally stable over this temperature range. Overall, the distinct shift in the TG-DTA profile for the 5-FU@COF composite compared to the pristine drug confirms the successful incorporation of the 5-FU within the COF's framework.

3.2. *Characterization of electrospun fibers*

The PLA/PEG fibers displayed smooth, continuous, bead-free morphology with an average diameter of 1047 ± 187 nm (Fig. 4a–b, Supporting Fig. S4a). COF/fibers and 5-FU@COF/fibers retained similar overall morphology but exhibited surface protrusions associated with embedded COF particles and a characteristic yellow tint consistent with the COF color (Supporting Fig. S5b-c). Their mean diameters decreased slightly to 944 ± 126 nm and 933 ± 171 nm, respectively (Fig. 4c–f, Supporting Fig. S4b–c), corresponding to reductions of ≈9.8% and 10.9% relative to PLA/PEG fibers. This modest decrease is attributed to increased jet charge density and partial disruption of chain entanglement by rigid, ionic COF particles, which promote additional jet stretching during electrospinning [33]. In contrast, the 5-FU/fiber sample exhibited a much finer fibrous structure with numerous spindle-like defects and surface crystallites (Fig. 4g-h). The crystalline deposits were attributed to recrystallized 5-FU, suggesting that the drug migrated out of the polymer jet and phase-separated during electrospinning, as evidenced by the phase separation of the precursor solution before electrospinning (Supporting Fig. S6). The average fiber diameter further decreased to 579 ± 104 nm (Supporting Fig. S4d), which is 44.7% smaller than that of the neat and COF-containing samples. This pronounced reduction in diameter likely arises from the addition of DMF to dissolve 5-FU, which increases the conductivity of the spinning solution together with phase separation that reduces the effective chain entanglement density. The combination of thin fibers, surface crystallites, and spindle-like irregularities highlights the strong incompatibility of directly blended 5-FU with polymer fibers without the presence of COFs.

FT-IR spectroscopy was employed to verify the successful incorporation of COF and 5-FU@COF into the fibers, as well as to identify possible interactions between the drug, COF, and polymer matrix. As shown in Fig. 5a-b, the PLA/PEG control fibers (denoted as fibers) displayed the expected peaks for PLA/PEG composites, which include the ester $C = O$ stretching at 1748 cm^{-1}, C–O stretching vibration at 1082 cm^{-1}, and -CH_3 asymmetric and symmetric stretching at 2995 and 2944 cm^{-1}. Additionally, -CH_3 bending modes were observed at 1452 and 1361 cm^{-1}, respectively. The same peaks were retained in both COF/fibers and 5-FU@COF/fibers, indicating that the incorporation of COF or drug-loaded COF did not alter the PLA/PEG chemical structure in the polymer matrix after electrospinning.

A new peak emerged at 1517 cm^{-1} in both COF/fibers and 5-FU@COF/fibers, corresponding to the $C = N$ stretching vibration of the TAPT-DFTA COF framework, indicating the presence of COF particles within the electrospun fibers. Most importantly, the 5-FU@COF/fibers exhibited a distinct amide band at 1655 cm^{-1}, consistent with the amide peak observed in 5-FU@COF before electrospinning. The shifting of this amide peak from 1645 cm^{-1} (free 5-FU) to 1655 cm^{-1} in both 5-FU@COF and 5-FU@COF/fibers suggests weakening in the hydrogen-bonding environment of 5-FU following encapsulation, as explained earlier.

The XRD spectra of fibers, COF/fibers, and 5-FU@COF/fibers are presented in Fig. 5c-d. The primary diffraction peak of the embedded

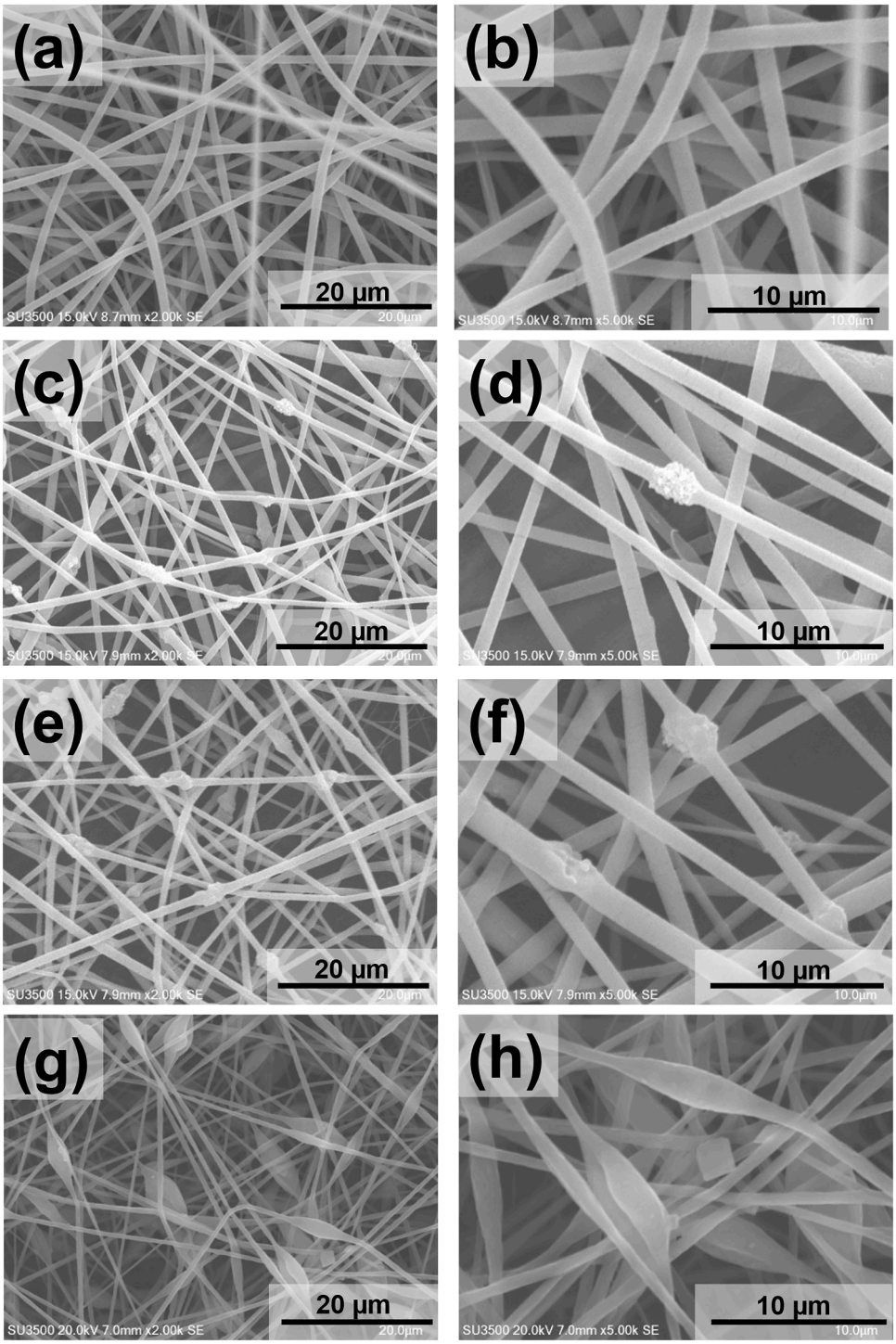

Fig. 4. SEM images of neat PEG/PLA fibers (a-b), 5-FU@COF/fibers (c-d), COF/fibers (e-f), and 5-FU/fibers (g-h) at 2000 and 5,000x magnification.

COF is clearly observed at around 2θ= 2.9°, with additional minor diffraction peaks at 3.1°, 5.0°, 5.8°, and 7.7° In addition, a diffraction peak at 2θ = 28.6° is observed for the 5-FU@COF samples, corresponding to the presence of 5-FU. For COF/fiber samples, only the main diffraction peak at 2θ=2.9 can be clearly observed, while the minor diffraction peaks appeared as a broader pattern, due to the lower content of COF in the sample. However, due to the nature of the amorphous PLA and low molecular weight PEG-1000 used to electrospun the fibers, no distinct peak can be found attributed to the polymer matrix other than a broad, amorphous region round 2θ = 18°-25°

The incorporation of COF and 5-FU@COF significantly influenced the mechanical behavior of the electrospun fibers, as summarized in Fig. 6a-c. The fibers exhibited the highest tensile strength (0.90 ± 0.04 MPa) and elastic modulus (0.09 ± 0.01 MPa) . Upon incorporation of COF, both tensile strength and modulus decreased to 0.69 ± 0.06 MPa and 0.04 ± 0.01 MPa, respectively, confirming that the presence of COF particles disrupted uniform chain packing and introduced weak sites within the COF/fibers. The 5-FU@COF/fibers sample exhibited the lowest mechanical performance among all samples, with a tensile strength of 0.55 ± 0.02 MPa and an elastic modulus of 0.03 ± 0.01 MPa., suggesting that loading 5-FU into the COF further weakened polymer–filler interactions, likely due to poorer interfacial adhesion or

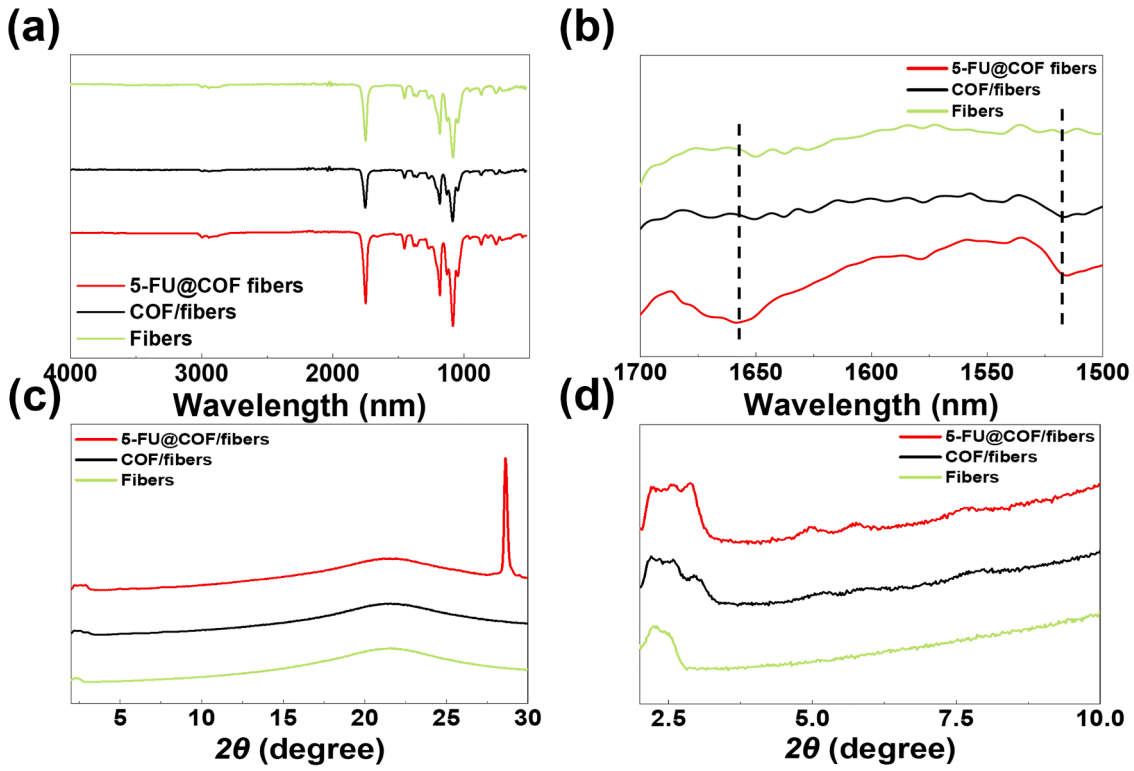

Fig. 5. FT-IR spectra (a-b) and XRD pattern (c-d) of the neat fibers, COF/fibers, and 5-FU@COF/fibers.

structural disruption caused by the encapsulated drug [34,35]. Despite the decreased mechanical strength, the mechanical properties of 5-FU@COF/fibers remain within the range reported for soft-tissue scaffolds, suturing, and topical drug delivery applications (0.2–1 MPa) [36–38].

The thermal properties of the fibers were analyzed using TGA and TG-DTG measurements and the results are presented in Fig. 6d-e and Supporting Table 1 . For the pristine fibers, the first degradation stage ($T_{d1,max}$= 323 °C) is attributed to the thermal degradation of the PLA matrix, while the second degradation stage ($T_{d2,max}$ = 392 °C) corresponds to the presence of PEG-1000 (Supporting Fig. S7 and Supporting Table 1) . Upon the incorporation of the COF, a pronounced enhancement in the thermal stability of the polymer composite was observed. For the COF/fibers, $T_{d1,max}$ shifted upwards to 360 °C, representing an increase of nearly 40 °C compared to the pristine fibers. . This enhancement indicates that the COF framework acts as a thermal barrier that delays the degradation of the composite.

A similar thermal degradation behavior was observed for the 5-FU@COF/fibers, which exhibited $T_{d1,max}$ and $T_{d2,max}$ values of 361 °C and 400 °C, respectively. No significant differences in $T_{d,max}$ values were observed between 5-FU@COF/fibers and COF/fibers, indicating that drug loading does not adversely affect the thermal stability imparted by the COF framework. Both COF-containing samples displayed a residual char fraction of approximately 3.8 wt.% at 700 °C, whereas the pristine fibers showed almost complete mass loss. This remaining char fraction is attributed to the thermally stable COF framework, which remains intact after the degradation of the polymer matrix. This observation further confirms the homogenous integration of the COF within the fiber scaffold. However, the $T_{initial}$ for 5-FU@COF/fibers decreased to approximately 200 °C due to the early degradation of the amorphous 5-FU confined within the COF's framework. Consequently, while the presence of COF framework significantly enhances the overall thermal stability of the fiber scaffold and the characteristic drop in $T_{initial}$ serves as a clear indicator of the successful loading of the amorphous drug within the fibers. Additionally, DSC thermograms (Fig. 6f) revealed endothermic peaks around 44–52 °C for all fiber samples. These peaks are attributed to the melting of PEG-1000 domains. In contrast, no distinct melting peak corresponding to PLA was detected, which is consistent with the amorphous nature of the PLA grade used. For 5-FU@COF/fibers, additional endothermic events were observed at 202.5 and 259.5 °C due to the melting of encapsulated 5-FU. The depression of 5-FU`s melting peak in the fibers compared to the melting temperature of crystalline 5-FU suggests that 5-FU is confined within the COF pores and polymer matrix, which can reduce their crystallinity and shift melting peaks to a lower value. This confinement-induced amorphization is consistent with the reduced $T_{initial}$ observed in TGA and confirms the successful loading of 5-FU without compromising the enhanced thermal stability imparted by the COF framework.

The surface wettability of the electrospun fibers was evaluated by static water contact angle measurements (Fig. 7). At 0 s, pristine PLA/PEG fibers, COF/fibers, and 5-FU@COF fibers have a water contact angle of 122.4 ± 0.9, 124.4 ± 0.2, and 118.4 ± 0.3, respectively, confirming their overall hydrophobic character (>90°) [39]. The incorporation of COF alone did not significantly alter surface hydrophobicity, whereas loading 5-FU@COF within the fibers slightly decreased their contact angle due to the presence of polar 5-FU. Furthermore, a gradual decrease in contact angle from 0 to 60 s was observed for all samples, which is attributed to the PEG-1000 segments that progressively interact with the water droplet and promote partial surface wetting over time.

3.3. Swelling behavior and degradation test

Fig. 8a showed the water-uptake of the fiber samples in pH 7.4 and pH 5.4. Pristine PLA/PEG fibers showed the highest swelling ratios of 413.3 ± 30.1% and 326.7 ± 15.2% at pH 7.4 and pH 5.4, respectively. In general, the high water uptake capacity is due to the presence of hydrophilic PEG-1000 that drives water adsorption into the fiber samples. The fibers exhibited a more pronounced water uptake at pH 7.4 compared to 5.4. The incorporation of COF into the fibers reduced the swelling ratio to 313.0 ± 15.3% at pH 7.4 and 300.0 ± 10.0% at pH 5.4,

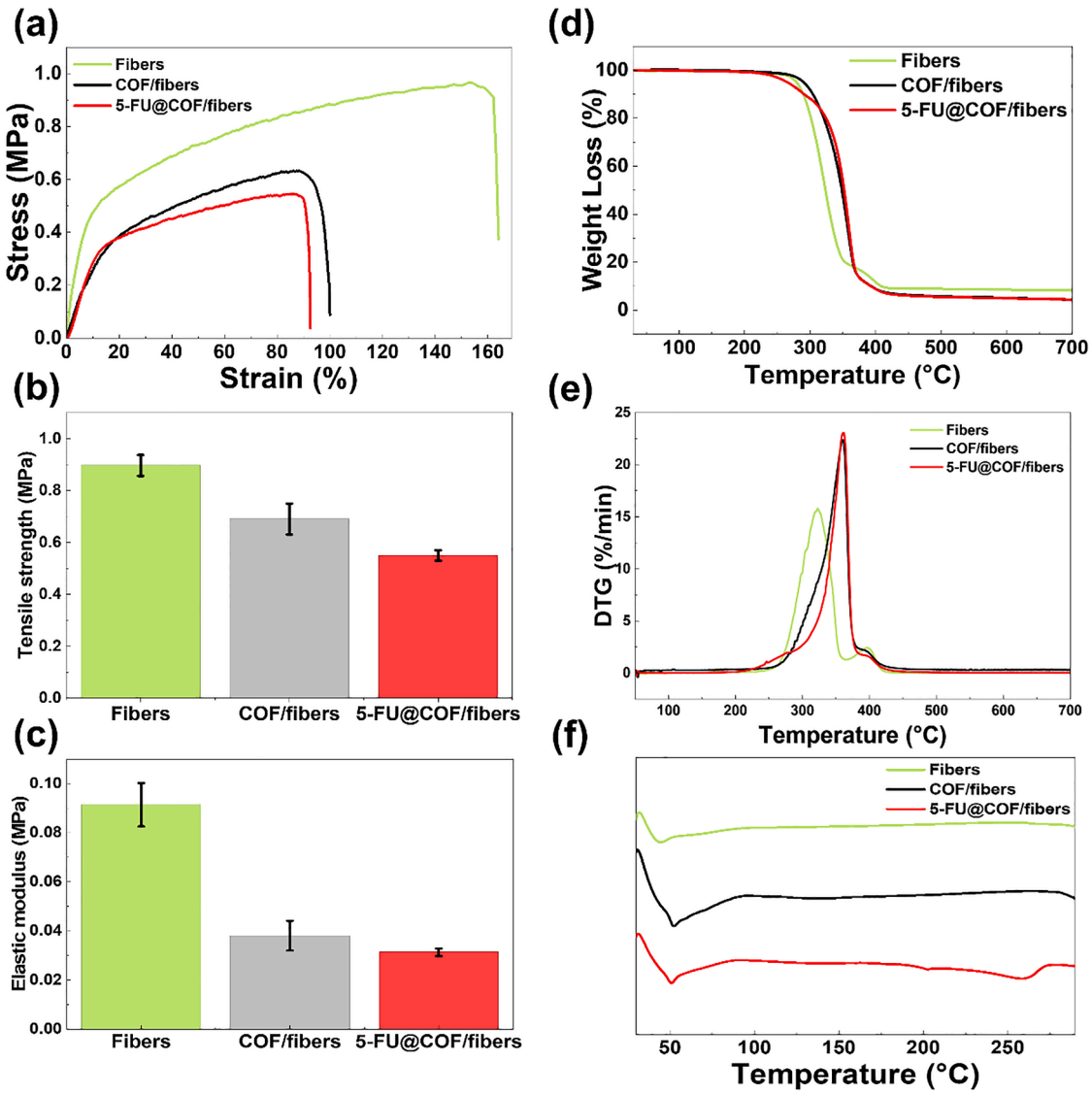

Fig. 6. Stress-strain curves (a) tensile strength (b) and elastic modulus (c) of the neat fibers, COF/fibers, and 5-FU@COF/fibers. TGA analysis (d) and DSC measurements (e) of the neat fibers, COF/fibers, and 5-FU@COF/fibers.

respectively. This results from the reduced free volume within the COF/fiber samples and the hydrophobic property of the COF particles, which in turn reduced water penetration [35]. The 5-FU@COF/fibers showed the lowest swelling (250.0 ± 20.0% at pH 5.4 and 226.7 ± 15.0% at pH 7.4), indicating that drug-loaded COF further limited water uptake capacity.

The degradation behavior of the 5-FU@COF/fibers were evaluated over the course of a week and their weight loss and structural degradation are studied after 1,4 and 7 days of immersion in PBS buffer at pH 7.4 and 5.4. As summarized in Fig. 8b, the fibers lost 5.1 ± 0.3 % of their weight in pH 7.4 buffer and 8.9 ± 1.0 % in pH 5.4 buffer. Based on the SEM images in Fig. 8c1 and c4, no significant differences in morphology were observed between these two fibers sample in terms of surface degradation or erosion. However, the samples lost a significantly higher weight in pH 5.4 buffer on day 4 (27.1 ± 2.5 %) and day 7 (36.7 ± 2.6 %), compared to pH 7.4, where the fibers only lost 6.3 ± 0.4 % and 7.7 ± 0.5 % of their weight, respectively. The SEM analysis revealed the presence of surface erosion and degradation after day 4 (Fig. 8 c2 and c5) and 7 (Fig. 8 c3 and c6,) at pH 7.4 and 5.4. Based on these results, the accelerated degradation can be attributed to PEG leaching in addition to the 5-FU released from the fibers, which are especially pronounced at a lower pH. The overall fiber degradation can be clearly observed in the SEM images of the fibers at a lower magnification (Supplementary Fig. S8) as well. These results also confirmed that the PEG progressively dissolves over time, contributing to the eroded fibers with beaded structure and rougher overall surface. Furthermore, the dissolution of PEG-1000 from the fibers plausibly occurred at a higher rate at acidic pH, which contributes to the lower apparent swelling observed in the fibers at pH 5.4. Consequently, the higher swelling at neutral pH reflect greater PEG retention within the fibers in comparison to those in acidic pH.

In addition to PEG dissolution, the observed mass loss at pH 5.4 exceeded the combined fraction of PEG and 5-FU@COF in the composite, indicating that the PLA matrix also underwent accelerated degradation under acidic conditions. Under standard physiological environments, PLA fibers electrospun from high-molecular-weight PLA typically degrade slowly through bulk hydrolysis over several weeks to months [2,40]. However, the incorporation of a low-molecular wright, hydrophilic compounds into PLA composite typically accelerates its degradation process [41]. The addition of low–molecular-weight PEG in PLA fibers significantly increased water uptake into the fibrous structure, providing an aqueous environment that facilitates accelerated

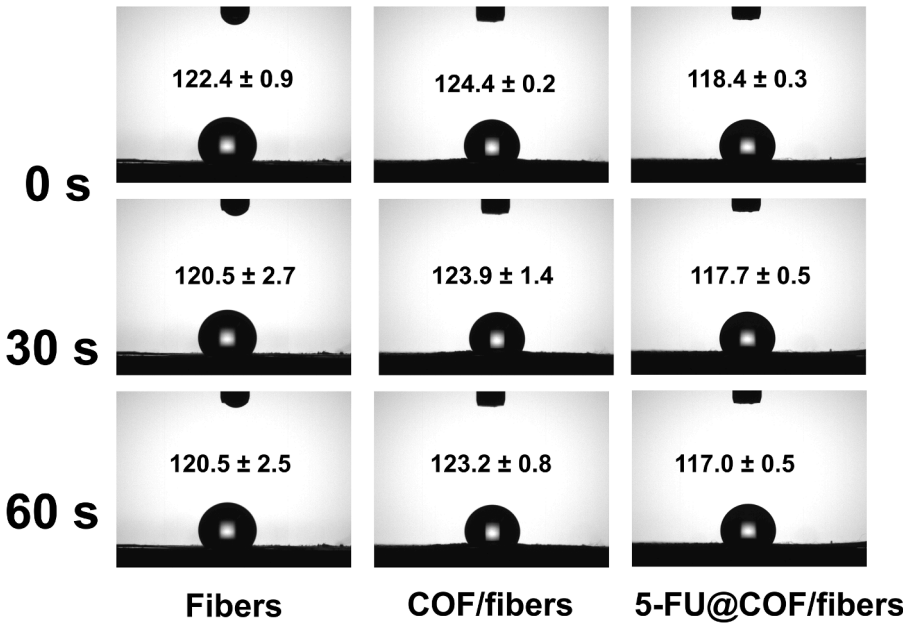

Fig. 7. Water contact angle measurements of neat PLA/PEG fibers, COF/fibers, and 5-FU@COF/fiber at 0,30, and 60 s.

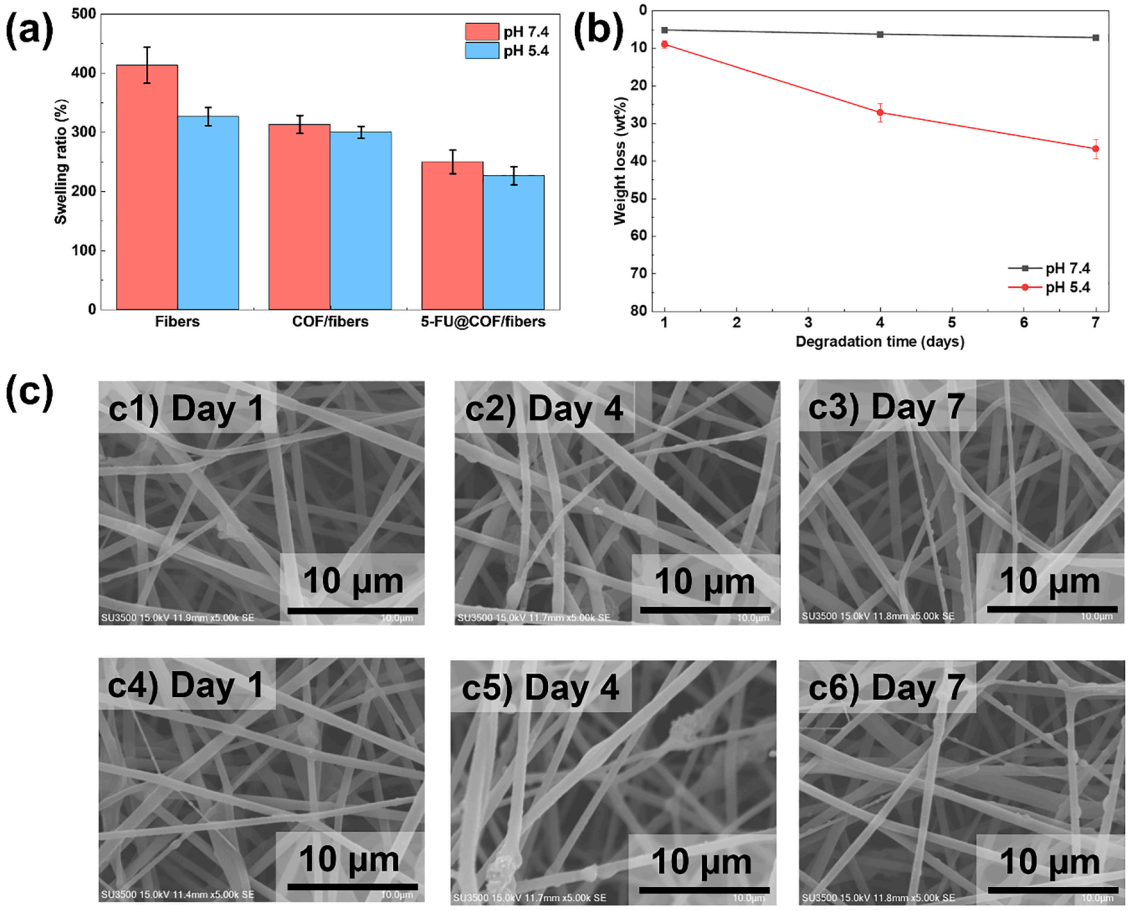

Fig. 8. Swelling ratio of neat PLA/PEG fibers, COF/fibers, and 5-FU@COF/fibers at pH 7.4 and pH 5.4 after 24 h (a). Weight loss of 5-FU@COF/fibers at pH 7.4 and 5.4 (b). SEM analyses of 5-FU@COF/fibers after degradation test at pH 7.4 (c1-c3) and pH 5.4 (c4-c6) at 5 000x magnification.

acid-catalyzed hydrolysis of ester bonds in PLA. Furthermore, fully amorphous PLA was used in this system. Unlike semicrystalline PLA, it lacks crystalline regions that are more resistant towards hydrolytic degradation. Consequently, hydrolysis proceeds more rapidly in the disordered amorphous regions, leading to accelerated degradation under acidic conditions [42]. Therefore, the combined effects of PEG

dissolution and enhanced hydrolytic degradation of the amorphous PLA matrix account for the accelerated fiber degradation observed under acidic conditions.

3.4. Drug release studies

The drug release profiles of 5-FU@COF/fibers and 5-FU/fibers in pH 7.4 and 5.4 was evaluated, and their cumulative drug release profiles are shown in Fig. 9. The total 5-FU content was quantified to be 6.15% wt% for 5-FU@COF/fibers and 8.05% wt% for 5-FU/fibers. Within the first 2 hours, 5-FU@COF/fibers exhibited an initial release of 26.5% at pH 7.4 and 38.6% at pH 5.4. Following this, a sustained release was observed up to 24 hours, at which point the cumulative release reached 48.9% and 71.9% for pH 7.4 and 5.4, respectively. Beyond 24 hours, the release profiles approached a plateau, ultimately reaching a maximum release of 64.5% at pH 7.4 and 90.0% at pH 5.4 after 168 hours (7 days).

To isolate the specific influence of the covalent organic framework (COF) on the drug release behavior, the drug release profiles of 5-FU@COF/fibers were compared against fibers directly loaded with the drug (5-FU/fibers). The 5-FU/fibers control showed limited early-stage 5-FU release, reaching only 9.53% at pH 7.4 and 11.6% at pH 5.4 within 2 h. After 24 h, drug release increased modestly up to 26.9% and 34.5% at pH 7.4 and pH 5.4, respectively. After 7 days, the cumulative release reached 33.0% at pH 7.4 and 43.5% at pH 5.4. The difference in release magnitude, particularly the nearly double cumulative release at pH 5.4 compared to the control fibers, demonstrates that the COF facilitates enhanced pH-responsive drug release from the fibrous scaffold.

Zeta potential measurements were conducted for both the COF and 5-FU@COF at pH 7.4 and pH 5.4 to probe the drug-carrier interactions, and the results are summarized in Table 2. For the drug-free COF, the surface charge shifted from -39.2 ± 2.4 mV (pH 7.4) to -35.5 ± 1.5 mV (pH 5.4), indicating only mild protonation of the imine linkages. In addition, 5-FU@COF exhibited only a slight increase in negative surface charge at pH 5.4 (-40.8 ± 3.0 mV) compared to pH 7.4 (-38.1 ± 2.3). Overall, both COF and 5-FU@COF exhibited comparable zeta potential values at both pH conditions and the absence of charge reversal upon drug loading suggests that 5-FU is predominantly physically adsorbed through non-electrostatic interactions such as hydrogen bonding, F-H bonding, and π–π stacking [43].

In the absence of significant electrostatic interaction between 5-FU and the COF that might influence release behavior, the enhanced drug release at pH 5.4 can be simply attributed to the structural degradation of the imine-linked COF framework under acidic conditions, as evidenced by XRD analysis in Supplementary Fig. S9. The imine linkage within the COF's framework are unstable under acidic conditions and can undergo a reversible reaction, leading to degradation [44]. At pH 7.4, the characteristic diffraction peaks of the COF remain discernible, although they exhibit peak broadening compared to the neat COF. In contrast, at pH 5.4, the diffraction peaks diminish significantly, indicating a substantial loss of crystalline structure. This confirms that the imine-linked framework is unstable under acidic conditions and as it breaks down, the confined 5-FU molecules are easily released.

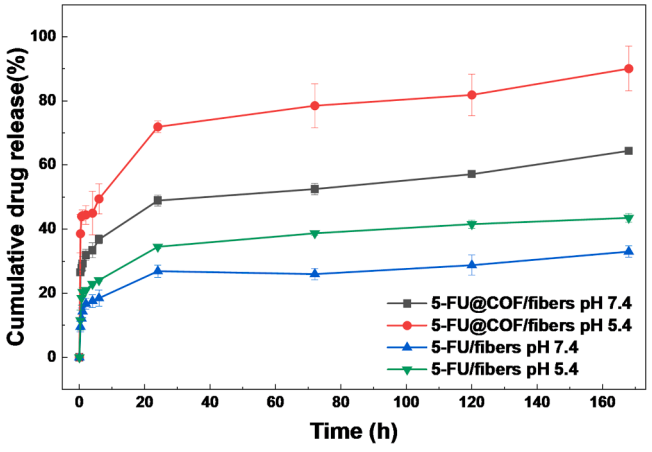

Fig. 9. Drug release profile of 5-FU from 5-FU@COF/fibers and 5-FU/fibers at pH 7.4 and 5.4.

Table 2
Zeta potential measurements of COF and 5-FU@COF.

pH	Sample	Zeta-potential (mV)
7.4	COF	-39.2 ± 2.4
	5-FU@COF	-38.1 ± 2.3
5.4	COF	-35.5 ± 1.5
	5-FU@COF	-40.8 ± 3.0

The degradation-induced drug release at acidic pH is further validated by the pH-sensitive release behavior of the 5-FU@COF particles (Supplementary Fig. S10). In the absence of a polymer matrix, the bare COF particles exhibited a rapid initial burst, releasing 48.1% at pH 7.4 and 59.3% at pH 5.4 in the first 2 h. By day 7, the free COF particles achieved near-complete desorption, reaching 97.7% and 100% release at pH 7.4 and 5.4, respectively. While the bare COF demonstrates high pH-responsive behavior, its high initial burst release makes it unfavorable for applications requiring sustained release. Embedding the 5-FU@COF into the PLA/PEG fibrous matrix successfully addresses this limitation by providing structural confinement that effectively reduce initial drug release. As shown in Fig. 9, the fibrous matrix suppressed the 2-hour burst to 26.5% (pH 7.4) and 38.6% (pH 5.4), nearly halving the initial release compared to the bare particles.

The drug release profiles were fitted to Higuchi, Korsmeyer-Peppas, and Weibull models and the corresponding kinetic parameters are summarized in Table 3 and Supplementary Fig. S11-S12. At pH 7.4, the data showed higher correlation with both the Korsmeyer–Peppas (R^2 = 0.983) and Weibull (R^2 = 0.988) models compared to Higuchi. The strong fit for the Korsmeyer–Peppas model with a release exponent n = 0.137, confirms that at physiological pH, the drug release is primarily governed by Fickian diffusion through the PLA/PEG fibrous network. However, a shift in kinetic behavior was observed under acidic conditions (pH 5.4). At this pH, the Korsmeyer-Peppas model provided an inadequate fit (R^2 = 0.707), indicating that the release no longer follows a simple diffusion process. In contrast, the Weibull model maintained the highest fit at (R^2 = 0.967). The scale parameter (α) dropped from 231.7 at pH 7.4 to 12.7 at pH 5.4, validating the accelerated release kinetics. Furthermore, the shape parameter (ß = 0.243) being less than 1 characterizes a parabolic release curve with a high initial rate, typical of complex systems experiencing a significant burst effect. The failure of standard diffusion models at lower pH highlights the transition to a multi-mechanistic process. In contrast to a simpler drug diffusion process at pH 7.4, the drug release mechanism at pH 5.4 further involves the pH-induced degradation of both PLA/PEG fibers and COF under acidic conditions, as explained in previous sections.

Overall, the introduction of 5-FU@COF into the fibers creates additional hydrophilic channels that enhance drug release through carrier degradation. On the other hand, in 5-FU/fibers, the drug tends to recrystallize and become trapped between denser fibers, resulting in

Table 3
Release kinetics parameter of 5-FU from 5-FU@COF/fibers at pH 7.4 and 5.4.

pH	Model	K	n	R^2	α	β
7.4	Korsmeyer-Peppas	3.23	0.137	0.983	N/A	N/A
	Higuchi	27.6	N/A	0.956	N/A	N/A
	Weibull	N/A	N/A	0.988	231.7	0.196
5.4	Korsmeyer-Peppas	3.66	0.092	0.707	N/A	N/A
	Higuchi	40.1	N/A	0.941	N/A	N/A
	Weibull	N/A	N/A	0.967	12.7	0.243

slower release. The enhanced release from the 5-FU@COF/fiber composite is driven by the degradation of imine-linked COF, along with the accelerated degradation of PLA/PEG fibers under acidic conditions. Thus, the COF do not merely act as a passive porogen; it contributes towards a dual-responsive effect, where both COF and polymer matrix respond cooperatively to enhance drug release under acidic conditions. Additionally, the polymer matrix plays a key role in modulating the release behavior of drug-loaded COF. Embedding the 5-FU@COF within the fibrous PLA/PEG structure introduces additional diffusion barriers that reduces drug burst release, which is useful in designing biopolymer composites with controlled release properties and improved pH-responsiveness.

4. Conclusion

Fluorinated covalent organic frameworks were successfully employed as compatibility-bridging carriers to incorporate the hydrophilic anticancer drug, 5-fluoruracil into hydrophobic electrospun PLA/PEG fibers. High encapsulation of 5-FU within the fluorinated COF (65%) improved drug dispersion within the polymer matrix and suppressed surface recrystallization of drug during electrospinning. Compared with free 5-FU@COF particles and directly loaded 5-FU fibers, the 5-FU@COF/fibers reduced the initial drug burst release and provided sustained, diffusion-controlled release over 7 days, with markedly higher cumulative release at pH 5.4 than at pH 7.4. This enhanced pH-responsive behavior arises from the combined effects of pH-induced COF degradation, combined with accelerated structural degradation of PLA/PEG fibers under acidic conditions. The integration of COFs into polymeric fibers not only modulates drug release but also alters the thermal degradation pathways of the fibers, indicating that the COF inclusion is a useful strategy to enhance the thermal stability of the polymer composite. . In addition, the prepared fibers displayed sufficient mechanical properties for soft-tissue scaffolds and topical drug delivery applications. Overall, these findings underscores the strong potential of 5-FU@COF/fibers as promising platform for anticancer drug delivery applications, thereby advancing the development of COF-polymer composites for sustainable biomedical applications.

CRediT authorship contribution statement

Hasinah Rafiq: Writing – original draft, Resources, Methodology, Investigation, Formal analysis, Data curation. **Yu-I Hsu:** Writing – review & editing, Visualization, Resources, Investigation, Funding acquisition, Conceptualization. **Mitsuharu Suzuki:** Writing – review & editing, Visualization, Methodology, Funding acquisition. **Supritha Muppuri:** Investigation. **Ken-Ichi Nakayama:** Visualization, Resources, Methodology. **Hiroshi Uyama:** Supervision, Funding acquisition.

Declaration of competing interest

The authors declare that they have no known competing financial interests or personal relationships that could have appeared to influence the work reported in this paper.

Acknowledgements

This work was supported by Japan Science and Technology Agency (JST) PRESTO Grant Number JPMJPR23N4, the Core Research for Evolutional Science and Technology (CREST) Program Grant Number JPMJCR24S5, the Environment Research and Technology Development Fund, Grant Number JPMEERF21S11900, the Environmental Restoration and Conservation Agency of Japan Grant Number JPMEERF20253G01, and Japan Society for the Promotion of Science (JSPS) KAKENHI Grants (22K21348 and 23K26717), and Japan Society for the Promotion of Science (JSPS) KAKENHI (Grant No. 24K01553). The first author would like to express her gratitude for the support of the Japanese Government (MEXT) Scholarship funded by the Ministry of Education, Culture, Sports, Science and Technology.

Supplementary materials

Supplementary material associated with this article can be found, in the online version, at doi:10.1016/j.polymdegradstab.2026.112065.

Data availability

No data was used for the research described in the article.

References

[1] J. Xue, T. Wu, Y. Dai, Y. Xia, Electrospinning and electrospun nanofibers: methods, materials, and applications, Chem. Rev. 119 (2019) 5298–5415, https://doi.org/10.1021/acs.chemrev.8b00593.
[2] E. Jaisankar, R.S. Azarudeen, M. Thirumarimurugan, Nanofibers embedded with nanoparticles as carriers for the controlled release of anticancer drug: promoting the apoptosis of breast cancer cell line and growth inhibition of microbial strains, ACS Appl. Bio Mater. 7 (2024) 4323–4338, https://doi.org/10.1021/acsabm.4c00183.
[3] J. Chen, R. Xuan, Y. Dou, C. Xu, T. Lu, Z. Jiang, D. Ding, C. Wang, J. Yan, B. Yang, Enhanced piezoelectric photocatalysis performance of polymers/P25 nanofibers on rhodamine b remediation via polar functional group engineering, ACS Appl. Polym. Mater. 6 (2024) 13671–13680, https://doi.org/10.1021/acsapm.4c02369.
[4] S. Zhang, X. Huang, W. Xiao, L. Zhang, H. Yao, L. Wang, J. Luo, J. Gao, Polyvinylpyrrolidone assisted preparation of highly conductive, antioxidation, and durable nanofiber composite with an extremely high electromagnetic interference shielding effectiveness, ACS Appl. Mater. Interfaces 13 (2021) 21865–21875, https://doi.org/10.1021/acsami.1c05319.
[5] T.M. Bradshaw, M.H. Schoenfisch, Properties of electrospun fibers that influence foreign body response modulation, ACS Biomater. Sci. Eng. 11 (2025) 55–66, https://doi.org/10.1021/acsbiomaterials.4c01143.
[6] S. Kumar, A.P. Singh, S. Senapati, P. Maiti, Controlling drug delivery using nanosheet-embedded electrospun fibers for efficient tumor treatment, ACS Appl. Bio Mater. 2 (2019) 884–894, https://doi.org/10.1021/acsabm.8b00735.
[7] X. Su, Y. Zhai, C. Jia, Z. Xu, D. Luo, Z. Pan, H. Xiang, S. Yu, L. Zhu, M. Zhu, Improved antibacterial properties of polylactic acid-based nanofibers loaded with ZnO-Ag nanoparticles through pore engineering, ACS Appl. Mater. Interfaces 15 (2023) 42920–42929, https://doi.org/10.1021/acsami.3c06791.
[8] F. Ebrahimi, H.Ramezani Dana, Poly lactic acid (PLA) polymers: from properties to biomedical applications, Int. J. Polym. Mater. Polym. Biomater. 71 (2022) 1117–1130, https://doi.org/10.1080/00914037.2021.1944140.
[9] L. Mou, J. Li, Y. Lu, G. Li, J. Li, Polylactic acid: a future universal biobased polymer with multifunctional performance—from monomer synthesis, and processing to applications: a review, J. Hazard. Mater. Adv. 18 (2025) 2772–4166, https://doi.org/10.1016/j.hazadv.2025.100757.
[10] S. Sahoo, W. Rathod, H. Vardikar, M. Biswal, S. Mohanty, S.K. Nayak, Biomedical waste plastic: bacteria, disinfection and recycling technologies—a comprehensive review, Int. J. Environ. Sci. Technol. 21 (2024) 1141–1158, https://doi.org/10.1007/s13762-023-04975-w.
[11] Jain MD Navami, La Beaud MD Desiree, How should US health care lead global change in plastic WasteDisposal? AMA J. Ethics® 24 (2022) 986–993.
[12] A. Samir, F.H. Ashour, A.A.A. Hakim, M. Bassyouni, Recent advances in biodegradable polymers for sustainable applications, Npj Mater. Degrad. 6 (2022) 68, https://doi.org/10.1038/s41529-022-00277-7.
[13] K.K. Gupta, N. Pal, P.K. Mishra, P. Srivastava, S. Mohanty, P. Maiti, 5-Florouracil-loaded poly(lactic acid)-poly(caprolactone) hybrid scaffold: potential chemotherapeutic implant, J. Biomed. Mater. Res. - Part A 102 (2014) 2600–2612, https://doi.org/10.1002/jbm.a.34932.
[14] M. Budai-Szűcs, A. Léber, L. Cui, M. Józó, P. Vályi, K. Burián, B. Kirschweng, E. Csányi, B. Pukánszky, Electrospun PLA fibers containing metronidazole for periodontal disease, Drug Des. Devel. Ther. 14 (2020) 233–242, https://doi.org/10.2147/DDDT.S231748.
[15] P.A. Haro Gutiérrez, S. Colombi, J. Casanovas, L. Resina, J. Sans, E. Engel, H. Enshaei, J. García-Torres, M.M. Pérez-Madrigal, C. Alemán, Engineering poly (lactic Acid)-based scaffolds for abundant, sustained, and prolonged lactate release, ACS Polym. Au 5 (2025) 247–260, https://doi.org/10.1021/acspolymersau.4c00097.
[16] L. Yi, S. Luo, L. Cui, M. Budai-Szűcs, J. Móczó, B. Pukánszky, Processes taking place during the preparation and use of electrospun PLA fibers and their effect on controlled drug release, J. Therm. Anal. Calorim. 147 (2022) 13191–13199, https://doi.org/10.1007/s10973-022-11554-7.
[17] H.J. Haroosh, Y. Dong, S. Jasim, S. Ramakrishna, Improvement of drug release and compatibility between hydrophilic drugs and hydrophobic nanofibrous composites, Materials. (Basel) 14 (2021) 1–17, https://doi.org/10.3390/ma14185344.
[18] A.L. Gürtler, T. Rades, A. Heinz, Electrospun fibers for the treatment of skin diseases, J. Control. Release 363 (2023) 621–640, https://doi.org/10.1016/j.jconrel.2023.10.009.

[19] N. Rajabifar, A. Rostami, S. Afshar, P. Mosallanezhad, P. Zarrintaj, M. Shahrousvand, H. Nazockdast, Wound dressing with electrospun core-shell nanofibers: from material selection to synthesis, Polymers. (Basel) (2024) 16, https://doi.org/10.3390/polym16172526.
[20] M. Habibi Jouybari, S. Hosseini, K. Mahboobnia, L.A. Boloursaz, M. Moradi, M. Irani, Simultaneous controlled release of 5-FU, DOX and PTX from chitosan/PLA/5-FU/g-C3N4-DOX/g-C3N4-PTX triaxial nanofibers for breast cancer treatment in vitro, Colloids Surfaces B Biointerfaces 179 (2019) 495–504, https://doi.org/10.1016/j.colsurfb.2019.04.026.
[21] M. Samy, B. Ekram, B.M. Abd El-Hady, M.M.H. Ayoub, In vitro release study of electrospun poly(ε-caprolactone)/gelatin nanofiber mats loaded with 5-fluorouracil, Polym. Bull. 81 (2024) 3953–3972, https://doi.org/10.1007/s00289-023-04930-2.
[22] S. Milenkova, M. Marudova, 5-Fluorouracil encapsulation in PLA films: the role of Chitosan particles in modulating drug release and film properties, Processes 13 (2025) 1–14, https://doi.org/10.3390/pr13071961.
[23] H. Mousazadeh, Y. Yazdani, Z. Mohammadi, V. Alivirdiloo, B. Nikzad, M. Mohammadzadeh, Fabrication of poly (lactic-co-glycolic acid)/mesoporous silica composite nanofibers for controllable co-delivery of 5-fluorouracil and curcumin against HT-29 colon cancer cells, J. Mater. Sci. 59 (2024) 2104–2120, https://doi.org/10.1007/s10853-023-09304-7.
[24] M.A. Alkhalifah, M. Yar, I. Bayach, N.S. Sheikh, K. Ayub, Covalent organic framework (C6N6) as a drug delivery platform for fluorouracil to treat cancerous cells: a DFT study, Materials. (Basel) 15 (2022) 7425, https://doi.org/10.3390/ma15217425.
[25] S. Das, Y. Zhao, T. Irie, J. Sakai, T. Sekine, H. Mabuchi, Y. Negishi, Three-dimensional covalent organic frameworks with pts topology for controlled anticancer drug delivery, (2023). https://chemrxiv.org/engage/chemrxiv/article-details/6426fb4d16782ec9e62304b9.
[26] M. Abbas, Z. Liang, M. Chen, W. Qu, S. Khan, M. Sameer, Toxicity challenges and current advancement in metal – organic frameworks (MOFs) for biomedical applications, (2025) 836–852. https://doi.org/10.1007/s12011-025-04712-z.
[27] B. Ma, Y. Xu, F. Hu, L. Zhai, Y. Huang, H. Qiao, J. Xiong, D. Yang, Z. Ni, X. Zheng, L. Mi, Fluorinated covalent organic frameworks for efficient drug delivery, RSC. Adv. 12 (2022) 31276–31281, https://doi.org/10.1039/d2ra05534a.
[28] J. Dong, W. Zheng, Y. Yang, S. Dong, S. Li, Y. Zhong, Y. He, Z. Cai, Z. Lin, Room-temperature synthesis of fluorinated covalent organic framework decorated superhydrophobic sponges for highly efficient crude oil spill cleanup, Sep. Purif. Technol. 344 (2024), https://doi.org/10.1016/j.seppur.2024.127314.
[29] C. Schlumberger, M. Thommes, Characterization of hierarchically ordered porous materials by physisorption and mercury porosimetry—a tutorial review, Adv. Mater. Interfaces 8 (2021) 1–25, https://doi.org/10.1002/admi.202002181.
[30] C.J. Doonan, D.J. Tranchemontagne, T.G. Glover, J.R. Hunt, O.M. Yaghi, Exceptional ammonia uptake by a covalent organic framework, Nat. Chem. 2 (2010) 235–238, https://doi.org/10.1038/nchem.548.
[31] S. Ayyanaar, R. Bhaskar, S. Esthar, M. Vadivel, J. Rajesh, G. Rajagopal, Design and development of 5-fluorouracil loaded biodegradable magnetic microspheres as site-specific drug delivery vehicle for cancer therapy, J. Magn. Magn. Mater. 546 (2022) 168853, https://doi.org/10.1016/j.jmmm.2021.168853.
[32] D.L. Melnikova, Z.F. Badrieva, M.A. Kostin, C. Maller, M. Stas, A. Buczek, M. A. Broda, T. Kupka, A.M. Kelterer, P.M. Tolstoy, V.D. Skirda, On complex formation between 5-fluorouracil and β-cyclodextrin in solution and in the solid state: ir markers and detection of short-lived complexes by diffusion nmr, Molecules. 25 (2020) 1–18, https://doi.org/10.3390/molecules25235706.
[33] J.Y. Zheng, M.F. Zhuang, Z.J. Yu, G.F. Zheng, Y. Zhao, H. Wang, D.H. Sun, The effect of surfactants on the diameter and morphology of electrospun ultrafine nanofiber, J. Nanomater. 2014 (2014) 1–9, https://doi.org/10.1155/2014/689298.
[34] C. Shen, Y. Ma, D. Wu, P. Liu, Y. He, K. Chen, Preparation of covalent organic framework-based nanofibrous films with temperature-responsive release of thymol for active food packaging, Food Chem. 410 (2023) 135460, https://doi.org/10.1016/j.foodchem.2023.135460.
[35] Y. Zou, P. Wang, A. Zhang, Z. Qin, Y. Li, Y. Xianyu, H. Zhang, Covalent organic framework-incorporated nanofibrous membrane as an intelligent platform for wound dressing, ACS Appl. Mater. Interfaces 14 (2022) 8680–8692, https://doi.org/10.1021/acsami.1c19754.
[36] U.A. Sezer, B. Aru, K. Ozturk, Y. Gizem, O. Sogut, T.A. Caglar, M.R. Bozkurt, Zero-valent iron nanoparticles containing nanofiber scaffolds for nerve tissue engineering, (2020) 1815–1826. https://doi.org/10.1002/term.3137.
[37] B. Pei, W. Wang, Y. Fan, X. Wang, F. Watari, X. Li, Fiber-reinforced scaffolds in soft tissue engineering, (2017) 257–268. https://doi.org/10.1093/rb/rbx021.
[38] Y. Tomar, N. Pandit, S. Priya, G. Singhvi, Evolving trends in nanofibers for topical delivery of therapeutics in skin disorders, 8 (2023) 18340–18357. https://doi.org/10.1021/acsomega.3c00924.
[39] M. Lao, Y. Wang, X. Li, J. Li, X. Ning, S. Yin, X. Deng, Effect of specific surface area and hydrophobicity of electrospun nanofibers on the sustained release performance of diclofenac sodium, Langmuir. 40 (2024) 15887–15896, https://doi.org/10.1021/acs.langmuir.4c01909.
[40] K.K. Abdullah, The influence of In vitro degradation on the properties of polylactic acid electrospun Fiber mats, 13 (2025) 1–20.
[41] A. Bogdanova, E. Pavlova, A. Polyanskaya, M. Volkova, E. Biryukova, G. Filkov, A. Trofimenko, M. Durymanov, D. Klinov, D. Bagrov, Acceleration of electrospun PLA degradation by addition of gelatin increases of and diameters, 24 (2023) 3535.
[42] C.S. Proikakis, N.J. Mamouzelos, P.A. Tarantili, A.G. Andreopoulos, Swelling and hydrolytic degradation of poly (D, L -lactic acid) in aqueous solutions, 91 (2006) 614–619. https://doi.org/10.1016/j.polymdegradstab.2005.01.060.
[43] N. Kaur, P. Tiwari, P. Kumar, M. Biswas, A. Sonawane, S.M. Mobin, Multifaceted carbon dots : toward pH-responsive delivery of 5 - fluorouracil for In vitro antiproliferative activity, 6 (2023) 2760–2770. https://doi.org/10.1021/acsabm.3c00228.
[44] T. Chen, W. Jiao, W. Zhu, H. Wang, S. Huang, X. Lin, J. Liu, H. Xu, C. Su, Designed synthesis of imine-linked 2D covalent organic frameworks with enhanced stability and functionality, 36 (2024) 7362–7369. https://doi.org/10.1021/acs.chemmater.4c01292.